Modular Dynamic Models Of Large Offshore Multi-Terminal DC (MTDC) Networks

R. Teixeira Pinto*
Electrical Power Processing Group
Technical University of Delft

P. Bauer*
Electrical Power Processing Group
Technical University of Delft

***Abstract* – Wind energy will continue to grow in Europe by means of the continent's climate and energy policies. As a result, more wind turbines will be progressively installed offshore. In addition, future offshore wind farms have a tendency to be larger in size and installed increasingly away from shore. Hence, the development of large offshore multi-terminal DC (MTDC) networks seems to be one of the best ways of integrating and sharing large amounts of offshore wind power between several European countries. This paper introduces how the correct choice for transnational grids architecture can impact its development and performance, and how modularity can help overcome problems related with the intrinsic complexity of such systems. Subsequently, modular dynamic models of the most important subsystems inside a MTDC network are presented and, after derivation of the models, a case study is carried out to assess the overall system behavior and performance.**

1 Introduction

There is no sign that current levels of energy consumption are going to be reduce in short or long terms. The demand for electricity, led primarily by developing countries, is projected to steeply increase worldwide due to economic and population growth. With the current policies worldwide energy consumption is projected to increase by 44% in the following years until 2035 [1]. In Europe, an average growing rate of 2% could, by 2050, result in a demand for electricity which is two times bigger than current consumption levels.

Without incentives for research and development of alternative forms of energy, together with governmental legislations and policies restricting the use of fuels that contribute to greenhouse effect and climate change, is not likely that the world's energy mix will change in the near future. As a matter of fact, with current policies and regulatory schemes, coal will remain as the most consumed fuel for electricity generation for the upcoming decades and until 2030 electricity generation by coal will constitute 32% of the whole global electricity generation mix [1].

However, as electricity needs rise in Europe, given its policies and regulatory schemes towards energy, there will be a higher necessity for exploring and allocating more renewable energy resources in comparison to other locations in the world. The EU Energy Policy of achieving 20% reduction in emission of greenhouse gases, 20% improvement in energy efficiency and having 20% of its primary energy consumption coming from renewable sources by 2020, places Europe as a world leader in the field of sustainable and renewable energy. Across a range of different technologies – e.g. biogas, biomass, solar, hydro, wave and wind – Europe could add circa 600 TWh in new renewable electricity power production towards 2020 [2].

Inside this renewable generation mix, wind energy will most definitively play an important role in Europe's climate and energy goals towards implementation of the 20-20-20 targets. By 2020, it is expected that circa 1/3 of all the renewable primary energy generation in Europe will come from electrical sources. Estimations foresee wind energy accounting for 1/3 of all renewable electricity generation and offshore wind farms representing 1/3 of all wind energy production share [3].

According to these expectations several European agents target 40-70 GW of installed offshore wind energy in Europe by 2020-2030 on the North and Baltic seas. The European Wind Energy Association (EWEA) foresees, for instance, that by the end of 2020 there will be circa 40 GW of installed offshore wind energy in Europe [3].

Since most of the offshore energy in Europe

*Electrical Power Processing Group, Technical University of Delft, 4 Mekelweg 2628CD Delft, The Netherlands. Emails: R.TeixeiraPinto@tudelft.nl, P.Bauer@tudelft.nl.

is to be installed in the Baltic or North Sea, the integration aspects of this offshore power to the different national electricity grids constitute a very important challenge for the power industry. The North Sea Transnational Grid (NSTG) project; led by the Energy Research Center of The Netherlands (ECN) in partnership with the Technical University of Delft, aims to investigate the best ways of integrating large scale offshore wind power by the construction of a transnational transmission grid in the North Sea.

2 System Architecture

The NSTG project, with its plan of interconnecting around 60 GW of offshore wind power between several countries in the North Sea, is a very ambitious project. Most likely any initiative of such dimension and complexity, it is extremely important right from the beginning to choose the most suitable architecture to allow the NSTG to organically grow with time from its initial phase; inherently simple, to its desired final form, hopefully with a much more complex topology, such as a meshed multi-terminal DC transmission (MTDC) system.

System architecture has several possible definitions. One way to evaluate the architecture of a system is to verify the way on which its operative elements are arranged into blocks and how these blocks interact. One of the most famous definitions on the matter is Ulrich's [4]: *"System architecture is the scheme by which the function of a system is allocated to physical components"*.

Hence, system architecture defines the way in which components inside a system interact and interface with each other. Regarding system architecture, one important aspect is the distinction among integral (or closed) and modular (or open) system architectures.

A system embracing an integrated architecture is commonly designed so as to maximize a particular performance measure; however, modifications to one feature or component may require extensive redesign of the whole system. Sometimes implementation of functional elements may be distributed across multiple components and eventually boundaries between these components may be difficult to identify or may not even exist.

Modularity Inside the NSTG

If one analyzes the complexity involved in the development of a system such as the NSTG, it is then immediate that an integrated architecture is evidently not the most convenient choice for the development and construction of the system. Modifications to features or components are likely to occur regularly during the initial and growing phases, however, there should be little, if any, redesign of the whole system given technical difficulties and vast costs involved.

For systems such as the NSTG, one possible solution is to adopt, already from the very early stages of development, a modular system architecture approach. A module is usually defined as a part of a system that is not so strongly coupled to other elements inside the system. Carliss gives a definition of modularity as [5]:*"Modularity is the practice of building complex systems or processes from smaller subsystems that can be designed independently yet function together as a whole".*

Such a modular architecture allows a change to be made to one module without generally affecting other modules. Each module may also be designed quite independently from each other.

Thus, in a project of such extent, it is somehow important to be able to distinguish clearly which are the objectives and primary functions of each system's modules and what are the possible interactions between these modules since than more than one stakeholder will be involved and needed for funding and development of the whole system.

Design Hierarchy

In the modularization process of a complex system, the first task is to establish which are the parts of the system that can be considered modules or subsystems. For instance, in an offshore transmission grid; wind farms, HVDC converter stations, DC transmission cables and potential protective systems naturally constitute the basic building blocks or modules. At the end of the system design process, the final step is to perform integration and testing of the complete system.

In a complex modular system, the design engineers are the ones responsible for establishing a set of design rules which accounts for:

1. System components: what are the system's modules and their roles;

2. Interfaces: description of how the modules inside the system are connected and interact with each other;

3. Test procedures: procedures that set the performance levels of a certain subsystem and allow for comparison between different versions of the same subsystem.

Therefore, in a modular system, the design hierarchy is composed of levels. The global design rules are at the highest level and not all modules inside the system can directly see them. At the next level are the modules interfaces, system integration and communication and, at the lower levels, the design parameters that concern only the modules themselves. An example of how a system design hierarchy for the NSTG could resemble is shown below.

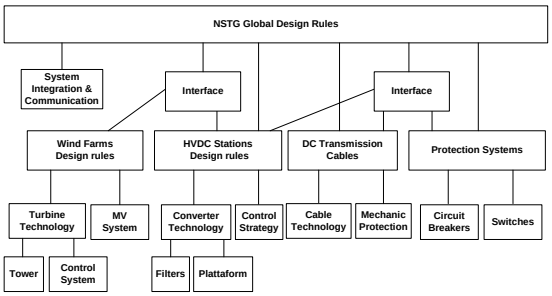

Figure 1: A possible design hierarchy for the NSTG system with four modules.

From the given NSTG system design hierarchy it is possible to see different levels of information access. In this case for example, the global design rules are directly visible to the HVDC Stations and to the Protection System modules but indirectly visible to Wind Farm modules.

This means that Wind Farm system engineers need only to take into account their local interface, i.e. the HVDC Stations modules, whilst engineers working on the latter have to take the system global design rules into consideration in addition to their local interfaces.

The NSTG global design rules, i.e. the design parameters in the top level of the diagram, must be established first due to the fact that they directly affect all the modules that are part of the system. Examples of global design rules inside the NSTG could include, but are not limited to, the DC voltage level in the MTDC system, the size of each HVDC Station and the power transfer capability of the DC cables.

During early development stages, the global design rules might appear simple or not complete. However, as the characteristics of the NSTG and the modules inside it become better understood, the design rules will also tend to be further developed.

The crucial point is that changes made in the global design rules will have large implications on all system modules, and are thus expected to be expensive and difficult to perform. In comparison, modifications of features inside a module, in the lower levels of the diagram, have limited extension, and should be then easier and cheaper to perform [5].

For instance, changing the DC voltage level of the MTDC system would be one of this far-reaching modifications that are bound to be costly and technically difficult [6]. Thus, once the DC level inside the NSTG system is establish, there will be very little room to change it. System engineers must carefully establish and take global design rules into consideration before systems like the North Sea Transnational Grid can be developed and built.

3 Dynamic Models of the NSTG Modules

Since, as previously discussed, a future NSTG would be build in a modular way, it is only natural that the models used to describe the system should also be modular in nature. Dynamic models of future large offshore multi-terminal DC networks are needed for assessment of the overall system behavior, during sound and fault conditions, but also for control designing purposes.

Modular dynamic models allow highly complex systems to be divided into smaller submodules. In that way, the complete system model can easier evolve with time and even allow for having different teams working in parallel in different modules inside the same system. In addition, using modular dynamic models makes it easier to perform comparative tests of individual modules performance.

To model large offshore transnational grids, the proposed approach is to derive mathematically the differential equations driving the dynamic models of the most important modules inside the system, viz.: wind farms, HVDC stations, the multi-terminal DC grid and the interconnected onshore AC systems. With this modular approach, it will be possible to study the dynamic behavior of MTDC networks irrespective of their topology.

3.1 MTDC Network

Multi-terminal HVDC (MTDC) transmission systems are characterized by more than two HVDC converter stations somehow interconnected on the DC side of the transmission system [7].

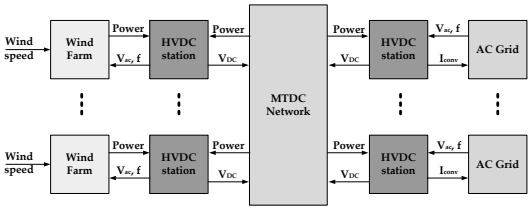

Figure 2: Modular representation of offshore MTDC networks.

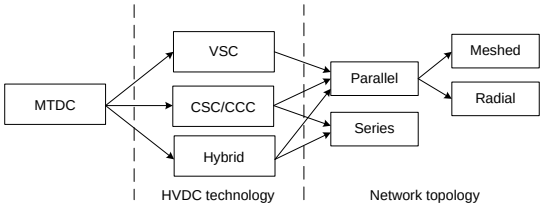

Figure 3: Classification of MTDC transmission systems.

The MTDC configurations can be classified according to the type of HVDC technology implemented at the converter stations, i.e.: line-commutated current-source converters (CSC) or forced-commutated voltage-source converters (VSC):

- CSC-MTDC: all the converter stations use the line commutated current-source converter HVDC technology;
- VSC-MTDC: all the converter stations use the forced-commutated voltage-source converter HVDC technology;
- Hybrid-MTDC: when both HVDC technologies (CSC and VSC) are used together.

Even thought there are over one hundred HVDC transmission systems installed all over the world, only three have more than two terminals: The Hydro-Québec/New England scheme, in Canada; the SACOI-2 scheme, between Italy and France [8]; and a back-to-back scheme using VSC technology at the Shin-Shimano substation, in Japan [9].

To form a multi-terminal transmission system the converters stations can be either connected in series or in parallel. When connected in series all the converter stations share the same current whilst for the parallel connection the converters share the same DC transmission voltage.

Given all the previously discussed characteristics, one possible way of classifying MTDC transmission systems would be according to the HVDC technology used and also according to the MTDC transmission system network topology. Figure 4 displays the proposed classification scheme.

In order to solve the electrical equations inside a MTDC network, it is necessary to know the DC voltage of all the nodes inside the system. Then, with knowledge of the DC voltages of all the HVDC stations it is possible to evaluate the DC current flowing in each of the transmission system's lines since:

$$\mathbf{I}_L = \mathbf{Y}(s) \cdot \mathbf{V_{DC}} \tag{1}$$

where $\mathbf{Y}(s)$ is the MTDC network admittance matrix, which is dependent on the topology of the MTDC grid.

After calculating the DC current in all lines of the MTDC system, the power flowing in the lines can be computed as:

$$P_L^n = I_L^n \cdot V_{DC}^n \tag{2}$$

where n is the station index number.

Figure 4: MTDC model block.

3.2 Voltage Source Converters

Given the characteristics of VSC-HVDC transmission systems it is most probable that this technology will be the one initially chosen for the connection of offshore wind farms since in offshore projects converter station footprint is a critical variable.

Modern state-of-the-art voltage-source converters for transmission purposes make use of modulation schemes or multilevel topologies, which allow them to have smaller space requirements than current-source converters. In addition, in VSC-HVDC stations there is no need for bulky special transformers, able to block DC voltages, as is the case for CSC-HVDC stations [8].

The VSC-HVDC model presented is modular and composed of several modules, viz.: a phase reactor, an inner current controller, the converter model, the outer controllers and the

station capacitor. The signal flow inside the VSC-HVDC model is displayed below.

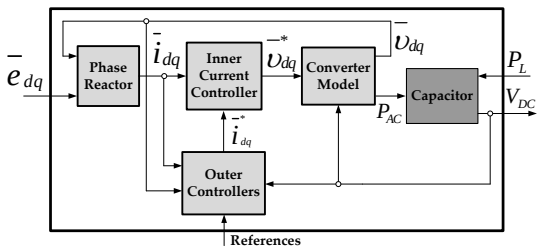

Figure 5: Modular representation of the VSC-HVDC transmission station.

3.2.1 Phase Reactor

A phase reactor is generally installed on the AC side of the VSC station. The reactor helps to further reduce AC high-frequency harmonic content, caused by the switching of the converter valves. In addition, independent control of active and reactive power is accomplished by regulating the voltage drop and current flow through the phase reactor on each converter station.

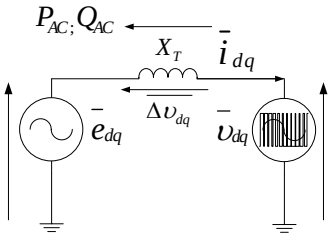

Figure 6: VSC-HVDC station single-phase equivalent circuit.

On the AC network side, the dynamics of the VSC-HVDC are modeled, in the rotating coordinate *(dq)* frame, by the following state-space equations:

$$\begin{cases} L_T \dfrac{d}{dt}(i_d) = e_d - \upsilon_d - R_T i_d + \omega L_T i_q \\ L_T \dfrac{d}{dt}(i_q) = e_q - \upsilon_q - R_T i_q - \omega L_T i_d \end{cases} \quad (3)$$

The resulting system is linear and autonomous, i.e. does not depend on time as an independent variable, if ω is constant. The poles of the system represented in (3) will be given by the roots of $(s + R_T/L_T)^2 + \omega^2 = 0$. For $\omega = 2\pi f$, where f is the AC network frequency (50 or 60 Hz), the poles of the non-feedbacked VSC system will be oscillatory. Moreover, without feedback of the converter currents the system would be poorly damped and have a very bad dynamic performance (under-damped response).

3.2.2 Inner Current Controller

The solution to improve the VSC system performance is to feedback the converter current through a controller closing the current loop.

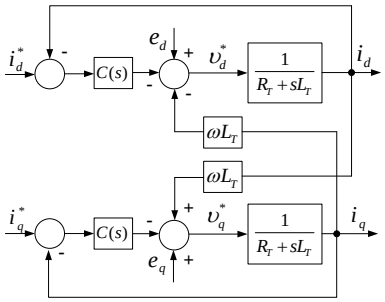

Figure 7: Block diagram representation of the VSC-HVDC state-space equations with feedback control.

Initially considering the controller to be a simple proportional gain, i.e. $C(s) = K_p$, the block diagram presented in Figure 7 can be simplified by solving the outer feedback loops. The transfer function of the outer feedback loops are given by:

$$\frac{K_p}{K_p + R_T + sL_T} \underbrace{\approx}_{K_p \gg R_T} \frac{1}{1 + sL_T/K_p} \quad (4)$$

With the assumption that $K_p \gg R_T$, the equivalent block diagram representation of the VSC-HVDC with the proportional controller becomes the one shown below in Figure 8.

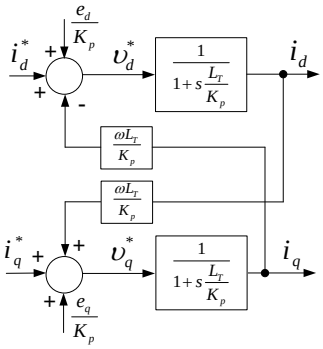

Figure 8: Equivalent block diagram representation of the VSC-HVDC with inner current controller.

With reference to the equivalent diagram it is possible to derive the following transfer function for the converter currents with respect to its reference values:

$$\frac{i_q}{i_q^*} = \frac{1 + s\frac{L_T}{K_p}}{\left(\frac{\omega L_T}{K_p}\right)^2 + \left(1 + s\frac{L_T}{K_p}\right)^2} \approx \frac{1}{1 + s\frac{L_T}{K_p}} \quad (5)$$

Therefore, having a sufficiently high proportional gain in the closed-loop controller not only improves the system response but also helps, in steady state, to eliminate the cross-coupled interaction between the d-axis and q-axis, and to reduce the effect of the grid side voltage variations on the converter current. Since during steady state s=0, it follows:

$$\begin{cases} \frac{i_q}{i_q^*} = \frac{1}{1 + \left(\frac{\omega L_T}{K_p}\right)^2} \approx 1 \\ \frac{i_q}{e_q} = \frac{\frac{1}{K_p}}{1 + \left(\frac{\omega L_T}{K_p}\right)^2} \approx \frac{1}{K_p} \\ \frac{i_q}{i_d^*} = \frac{\frac{\omega L_T}{K_p}}{1 + \left(\frac{\omega L_T}{K_p}\right)^2} \approx \frac{\omega L_T}{K_p} \end{cases} \quad (6)$$

In fact, if $\omega L_T/Kp \ll 1$, the cross-coupling influence of the axes are canceled out. Thus, starting from the oscillatory system of (3), by adding a proportional controller and closing the current-loop, the VSC-HVDC system now resembles two first-order systems (one for each axis) with poles in $-K_p/L_T$, which is the closed-loop bandwidth, α_c, of the system.

For a satisfactory dynamic performance, when using carrier-based PWM or space-vector PWM modulation techniques, the closed-loop bandwidth of the system should not be higher than 5 times the angular switching frequency and the switching frequency should not be lower than half the sampling frequency [10][11]; i.e. $\alpha_c \leq \omega_{sw}/5 \leq \omega_s/10$.

Hence, with a switching frequency of 2 kHz the maximum system bandwidth would be of approximately 2.5 krad/s. Given the fact that in a first-order system the rise-time, t_r, relates to the bandwidth, α_c, by the formula $\alpha_c = ln(9)/t_r$; the minimum current rise-time of the VSC, for a switching frequency of 2 kHz, would be of little less than *1 ms*.

In this way, the value of the proportional gain, K_p, is fixed by the obtainable bandwidth which, in the other hand, is related to the converter switching frequency. It follows that, in the VSC model, in order to obtain the desired closed-loop bandwidth it is necessary to make $K_p = \alpha_c L_T$.

Nevertheless, the proportional gain is limited and cannot be made higher due to the switching frequency limitation, hence, there will be a small error in the inner current controller, equal to $(\omega L_T/K_p)^2$, in steady state.

To cancel the steady-state error the solution is to use a PI regulator instead. In this case the inner current controller generates the *(dq)* reference voltages for the VSC-HVDC modulator as:

$$\begin{cases} v_d^* = e_d - \left(K_p + \frac{K_i}{s}\right)(i_{cd}^* - i_{cd}) - \omega L_T i_{cq} \\ v_q^* = e_q - \left(K_p + \frac{K_i}{s}\right)(i_{cq}^* - i_{cq}) + \omega L_T i_{cd} \end{cases} \quad (7)$$

As the steady-state error is of only a few percent, the integrator gain of the PI regulator, K_i, can and should be kept very low.

3.2.3 Converter Model

The next block inside the dynamic model of the VSC-HVDC system is the model of the voltage-source converter itself. As previously discussed, since the closed-loop bandwidth of the current controller is usually kept at least 5 times higher than the switching frequency of the modulator, its dynamic behavior can be neglected when evaluating the dynamic response of MTDC systems as a whole.

For this reason usually the average model of the converter is used, i.e.:

$$\begin{cases} v_d(k+1) = v_d^*(k) \\ v_q(k+1) = v_q^*(k) \end{cases} \quad (8)$$

where one time-step delay is introduced due to the controller computational time and also due to the converter blanking time [12].

Nevertheless, a more detailed switching model of the converter may be of interest when commutation losses, switching harmonics or ripple in the converter currents need to be taken into consideration. The mathematical description of modulated converter voltages in the 3-phase frame is given by:

$$v_{ci} = \frac{1}{2}\left(\delta_i(t) - \frac{1}{3}\sum_{i=a,b,c}\delta_i(t)\right)V_{DC}(t) \quad (9)$$

where δ_i is the switching function of phase i, generated by the modulator.

3.2.4 VSC-HVDC Station Capacitor

On the DC side, the VSC-HVDC station is usually represented by a controllable current source, acting on the station capacitor, as represented in Figure 9. The DC voltage of the VSC station and the power flowing into the DC network are then given by:

$$\begin{cases} W_{DC}^{n} = \int \left(P_{DC}^{n} - P_{L}^{n}\right) dt \\ V_{DC}^{n} = \left(\dfrac{2}{C_n} \cdot W_{DC}^{n}\right)^{\frac{1}{2}} \end{cases} \tag{10}$$

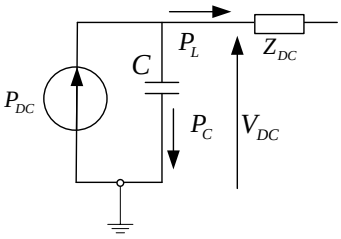

Figure 9: Equivalent circuit of the VSC-HVDC station DC side.

3.2.5 Outer Controllers

The outer controllers are the ones responsible for providing the current references signals for the inner current controller. For the VSC-HVDC there are basically two categories of outer controllers: the ones related with the active power and those with the reactive power.

The expressions to evaluate the active and the reactive power flowing through the converter, in the *(dq)* frame, are given as:

$$\begin{cases} p_{ac} = e_d \cdot i_d + e_q \cdot i_q \\ q_{ac} = e_q \cdot i_d - e_d \cdot i_q \end{cases} \tag{11}$$

If, under steady state conditions, the q-axis of the *(dq)* frame is assumed to be aligned with the AC network voltage phasor, i.e. $e_d = 0$, the active-power related controllers will provide i_q^* whilst the reactive-power ones will provide i_d^*.

The following equations give the references values for the reactive-channel outer controllers:

$$\begin{cases} i_d^* = (q_{ac}^* - q_{ac}) \cdot \left(K_{pq} + \dfrac{K_{iq}}{s}\right) \\ i_d^* = (|e_{dq}^*| - |e_{dq}|) \cdot \left(K_{pv} + \dfrac{K_{iv}}{s}\right) \end{cases} \tag{12}$$

Consistently, the active-channel outer controllers are given by:

$$\begin{cases} i_q^* = (p_{ac}^* - p_{ac}) \cdot \left(K_{pp} + \dfrac{K_{ip}}{s}\right) \\ i_q^* = (W_c^* - W_c) \cdot \left(K_{pw} + \dfrac{K_{iw}}{s}\right) \end{cases} \tag{13}$$

In all the outer controllers PI regulators are employed to annul steady-state errors.

As it can be noticed, the DC-voltage outer controller is made to operate on the error of the energy stored in the capacitor, $\Delta W_c = W_c^* - W_c$, instead of directly on the direct voltage. In the later case the system would be non-linear and the closed-loop dynamics of the DC voltage controller would be dependent on the operating point [13].

The outer controllers must have slower dynamics than the inner current controller. For stability reasons, a rule of thumb is that the outer controllers bandwidth should be kept smaller than at least 10% of the current controllers bandwidth [13]. Thus, for a switching frequency of 2 kHz, the maximum bandwidth of the outer controllers would be of approximately 250 rad/s. Subsequently, the outer controller regulator gains can be chosen to provide the desired bandwidth.

3.3 Wind Turbines

Modern wind turbines, with relatively high power ratings, are now build as variable-speed pitch-controlled turbines whilst in the past most wind turbines were fixed-speed stall-controlled units.

The electric generators inside wind turbines can be connected to the turbine shaft through a staged gearbox or be directly driven. As far as the generator type is concerned, wind turbines can be classified as: squirrel-cage induction generators (SCIG); doubly-fed induction generators (DFIG) and permanent-magnet synchronous generators (PMSG).

One of the goals inside the NSTG is to achieve the maximum aerodynamic efficiency as possible over a wide range of wind speeds. Therefore, it is most likely that PMSG types of wind turbines will be employed, given the fact they offer a higher range of dynamic speed control than DFIG ones, even though the later still constitutes the most used and marketed type of wind turbines.

3.3.1 Turbine Model

The turbine model is based on the mathematical expression of the mechanical power the

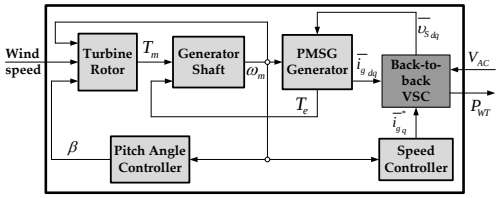

Figure 10: Modular representation of variable-speed PMSG wind turbines.

wind turbine generates from a given wind speed (ω_w). The available mechanical power (P_m) is defined as the power contained in the wind passing through the rotor area (A_r) multiplied by the power coefficient $(C_p(\lambda,\beta))$ which yields [14]:

$$P_m = \frac{T_m}{\omega_m} = \frac{\rho}{2} A_r \omega_w^3 C_p(\lambda,\beta) \tag{14}$$

while the power coefficient $C_p(\lambda,\beta)$ is calculated as [14]:

$$\begin{cases} C_p(\lambda,\beta) = 0.22\left(\dfrac{116}{\lambda_i} - 0.4\beta - 5\right) e^{\dfrac{-12.5}{\lambda_i}} \\ \dfrac{1}{\lambda_i} = \dfrac{1}{\lambda + 0.08\beta} - \dfrac{0.035}{\beta^3 + 1} \end{cases} \tag{15}$$

3.3.2 PMSG Model

The permanent-magnet synchronous generator model is based on the machine's magnetic, electric equations written in the rotating *(dq)* frame [15]:

$$\begin{cases} \overline{\lambda}_{dq} = L_{eq}\overline{i}_{dq} + \overline{\lambda_m}_{dq} \\ \overline{v_s}_{dq} = R_s\overline{i}_{dq} + \dfrac{d\overline{\lambda}_{dq}}{dt} + j\omega_r\overline{\lambda}_{dq} \end{cases} \tag{16}$$

The PMSG control strategy used is the field oriented control, where the permanent-magnet flux, $\overline{\lambda_m}_{dq}$, is aligned with the d-axis of the rotating frame so that $\overline{\lambda_m}_d = \lambda_m$ and $\overline{\lambda_m}_q = 0$. Substituting the obtained values of $\overline{\lambda_m}_{dq}$ in (16) and solving for the current derivatives yields the PMSG state-space equations:

$$\begin{cases} L_{eq}\dfrac{d}{dt}(i_d) = \upsilon_{sd} - R_s i_d + \omega_r L_{eq} i_q \\ L_{eq}\dfrac{d}{dt}(i_q) = \upsilon_{sq} - R_s i_q - \omega_r L_{eq} i_d - \omega_r \lambda_m \end{cases} \tag{17}$$

where ω_r is the electrical speed of the generator rotor, λ_m is the flux of the permanent magnet and, $L_{eq} = L_s + L_\sigma$, is the sum of the stator windings self-inductance and dispersed inductance.

As was the case for the VSC-HVDC state-space equations, the poles of (17), given by the roots of $(s + R_s/L_{eq})^2 + \omega_r^2 = 0$, are oscillatory and progressively less damped as ω_r increases. The solution is once more to feedback the stator currents through a current controller closing the current loop, a function that is accomplished by the current controller of the back-to-back converter inside the turbine. The current feedback is also important to guarantee that the rotor flux is aligned with the d-axis of the rotating reference frame by imposing $i_d^* = 0$, while the q-axis current reference (i_q^*) will come from the speed controller.

3.3.3 Speed Controller Model

The speed controller model is based on the generator shaft equation and on the fact that the q-axis current will control the electric torque since:

$$\begin{cases} T_e = \overline{\lambda}_{dq} \times \overline{i}_{dq} = \lambda_m i_q \\ \dfrac{d}{dt}\omega_r = J_g(T_e - T_m) \end{cases} \tag{18}$$

Thus, using a PI regulator for the speed controller, the reference torque can be calculated as:

$$T_e^* = i_q^* \lambda_m = \left(K_{ps} + \frac{K_{is}}{s}\right)(\omega_r - \omega_r^*) \tag{19}$$

4 Case Study

In order to test the described models and observe their behavior when connected altogether, a 4-node VSC-MTDC network composed of two AC grids and two Wind Farms is studied. The network is parallel-radial connected and its layout is shown below in Figure 11.

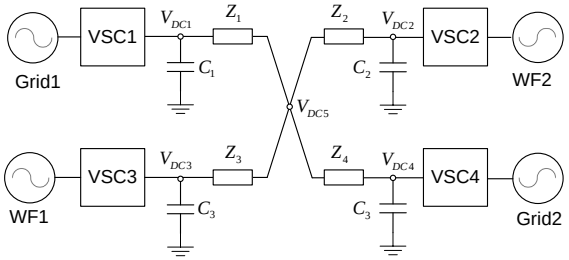

Figure 11: MTDC Network with 4 nodes.

The AC grids are modeled as ideal voltage sources behind short-circuit impedance and the wind farm model is obtained by proportionally scaling the power of the single PMSG by the number of wind turbines inside the wind farm. The MTDC data set used for the numeral simulation is displayed in Table 2 in the Appendix.

Initially the system is in steady-state, with no power flowing through the MTDC network, and all the voltages at The DC nodes are at 1 pu. The VSC-HVDC of AC Grid 1 is given the role of controlling the DC voltage inside the MTDC network whilst the other nodes are set for controlling their active power.

In order to assess the dynamics of the active power and of the DC voltages in the MTDC network the following order of events is considered: at simulation time t = 0.5s, the AC grid 2 starts requesting 1 pu power from the MTDC network; then, wind farm 1 starts producing 0.8 pu at t = 1.5s while wind farm 2 does the same but starting at t = 2.0s. Finally, at t=2.5s, VSC-Station 2 becomes inoperable due to a solid 3-phase fault happenning at AC grid 2. The active power flow in the MTDC network is depicted in Figure 12 while the DC voltage at the converter nodes is displayed in Figure 13.

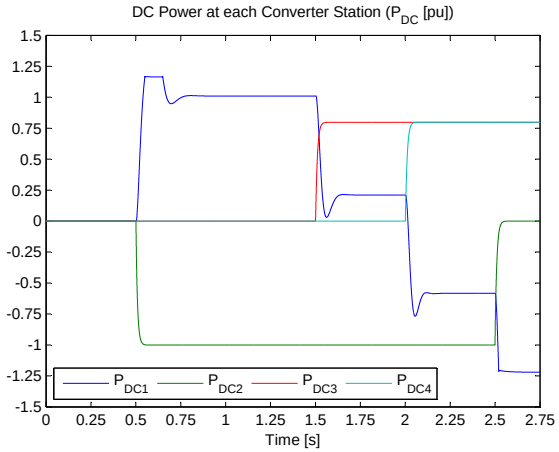

Figure 12: Active power inside the MTDC network.

In the VSC-HVDC Station 1 the current is rated at 1.2 pu to allow extra room for controlling the DC voltage inside the MTDC network. Nevertheless, this does not keep VSC1 power from saturating when AC Grid 2 starts asking for power. During this first transient, while the DC voltage of Station 1 falls to a little over 0.8 pu, in the other stations the DC voltage is kept above 0.9 pu. Since a 1 pu step in power is a demanding situation for the DC controller, it is possible to say that the MTDC system can cope with changes in the operating point within reasonable time (approx. 250 ms) while maintaining safe transient levels of the DC voltage ($\pm$ 0.2 pu).

However, the same cannot be stated for the fault scenario. When AC Grid 2 becomes

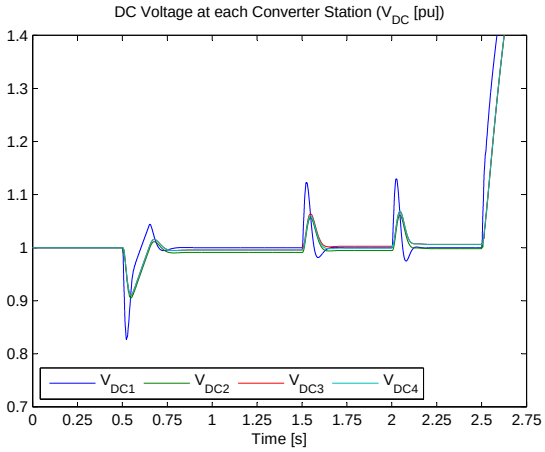

Figure 13: DC Voltages inside the MTDC network.

faulted there is an active power surplus in the MTDC network since the wind farms are producing 1.6 pu and the DC voltage controlling station can only handle a little over 1 pu.

In this work no LVRT technique is employed in order to assess how fast will the DC voltage rise in such fault cases. Figure 13 shows that the DC voltage of Station 1 reaches 1.3 pu in 55ms ($<$ 3 cycles) and 1.4 pu in 86ms ($<$ 5 cycles).

For the same fault scenario, Table 1 shows the time it would take for the DC voltage at Station 1 to reach 1.3 pu (and 1.4 pu) as a function of the DC power mismatch and the VSC-HVDC station capacitor size.

Table 1: DC Voltage Transient Time.

Time to $V_{DC1} = 1.3$ pu [ms]		
Power Mismatch [pu]	C = 75μF	C = 150μF
0.6	55	155
0.8	35	95
1.0	26	65
Time to $V_{DC1} = 1.4$ pu [ms]		
Power Mismatch [pu]	C = 75μF	C = 150μF
0.6	86	233
0.8	55	145
1.0	36	102

5 Conclusions

The construction of multi-terminal DC networks for integration of large-scale offshore wind power will probably happen modularly and, with time, these grids will grow both in size and complexity. However, the global design rules of such systems - e.g. the DC voltage level inside the MTDC network - must be carefully established

beforehand. Changes in the design rules on a later stage are expected to be both expensive and difficult to perform.

In this paper, modular dynamic models of the most important modules inside future MTDC systems were presented. It was shown that the DC side of offshore networks have very fast dynamic phenomena. During fault conditions, the DC voltage can reach unsafe values within only a few cycles of the AC network; thus, almost instantaneous reaction of the controls and protective schemes will be necessary in MTDC systems to maintain operation during contingencies.

Appendix

Table 2: MTDC Data used in the Simulations.

MTDC System Parameters		
AC Grids	Nominal Voltage	230 kV
	Frequency	50 Hz
	Short-Circuit Power	3000 MVA
VSC Stations	Nominal Power	400 MW
	Nominal AC Voltage	180 kV
	Nominal DC Voltage	$\pm$200 kV
	ICC Bandwidth	2 krad/s
	Phase Reactor	0.15 pu
	Station Capacitor	75 μF
Wind Farms	Nominal Power	400 MW
	Nominal Voltage	180 kV
	Turbine Power	5 MW
	Generator Voltage	1.2 kV
	PMSG flux λ_m	3.8 Wb
	PMSG Stator L_s	0.6 mH
	PMSG Stator L_σ	0.4 mH
	PMSG Stator R_s	14.7 mΩ
DC Network	Nominal Voltage	$\pm$200 kV
	DC cable Resistance	0.02 Ω/km
	DC cable Reactance	0.06 Ω/km
	DC lines length	100 km

References

[1] International Energy Agency, "World Energy Outlook," 2010.

[2] T. Gjengedal, "Future North Sea Grid and very high power wind farms in the North Sea," *EPE Wind Energy Seminar 2010 Stafford, UK*, p. Keynote Speech Presentation.

[3] European Wind Energy Association, "Oceans of Opportunity," 2009.

[4] K. T. Ulrich and S. D. Eppinger, *Product Design and Development*, vol. 384 of *McGraw-Hill/Irwin series in marketing*. McGraw-Hill, 1995.

[5] Y. Carliss, C. Y. Baldwine, and B. Clark, *Design Rules: The Power of Modularity*. MIT Press, 2000.

[6] E. Koldby and M. Hyttinen, "Challenges on the Road to an Offshore HVDC Grid," *Proc. Nordic Wind Power Conference*, 2009.

[7] Cigré, "VSC Transmission," *Working Group B4.37*, p. 162.

[8] J. Arrillaga, Y. H. Liu, and N. R. Watson, *Flexible power transmission: the HVDC options*. John Wiley and Sons, 2007.

[9] T. Nakajima and S. Irokawa, "A Control System for HVDC Transmission by Voltage Sourced Converters," in *IEEE Power Engineering Society Summer Meeting*, (Edmonton, Alta), pp. 1113–1119, 1999.

[10] L. Harnefors and H.-P. Nee, "Model-Based Current Control of AC Machines Using the Internal Model Control Method," *IEEE Transactions on Industry Applications*, vol. 34, no. 1, pp. 133–141, 1998.

[11] M. Kazmierkowski, R. Krishnan, and F. Blaabjerg, *Control in Power Electronics*. Academic Press, 2002.

[12] N. Mohan, T. M. Undeland, and W. P. Robbins, *Power Electronics: Converters, Applications and Design*. Wiley, 1995.

[13] L. Harnefors, M. Bongiorno, and S. Lundberg, "Input-Admittance Calculation and Shaping for Controlled Voltage-Source Converters," *IEEE Transactions On Industrial Electronics*, vol. 54, pp. 3323–3334, Dec. 2007.

[14] J. Slootweg, H. Polinder, and W. Kling, "Dynamic modelling of a wind turbine with doubly fed induction generator," in *2001 Power Engineering Society Summer Meeting*, pp. 644–649, Ieee, 2001.

[15] P. Kundur, N. J. Balu, and M. G. Lauby, "Kundur - Power System Stability and Control.pdf," 1994.

Biographies

Rodrigo Teixeira Pinto was born in *São Paulo*, Brazil, on November 3rd 1983. In 2003 he joined the *Escola Politécnica da Universidade de São Paulo* for a bachelor in Electrical Engineering at the Electrical Energy and Automation (PEA) department. In 2006 he started his MSc. in Electrical Engineering at the *Politecnico di Torino*, in Turin, Italy. From May to November 2008 he was with Siemens PTI, in Erlangen, Germany, working towards his MSc. as a *Diplomand* on the Network Dynamics Studies department. On December 2008 he received his MSc. (cum laude) from the *Politecnico di Torino*. Since December 2009 he is working as a PhD researcher on the North Sea Transnational Grid research project at the Electrical Power Processing group (EPP) of TU Delft.

Pavol Bauer received his Masters in Electrical Engineering at the Technical University of Kosice ('85), Ph.D. from Delft University of Technology ('95) and title prof. from the president of Czech Republic at the Brno University of Technology (2008). Since 1990 he is with Delft University of Technology, teaching Power electronics and Electrical Drives. From 2002 to 2003 he was working partially at KEMA (Arnhem) on different projects related to power electronics applications in power systems. P. Bauer published over 50 journal and 200 conference papers in his field, he is an author or co-author of 6 books, he holds international patent and organized several tutorials at the international conferences. He has worked on many projects for industry concerning wind power, power electronic applications for power systems such as Smarttrafo etc. and participated in several Leonardo da Vinci EU projects as project partner (ELINA, INETELE) and coordinator (PEMCWebLab.com). He is a Senior Member of the IEEE, Chairman of Benelux IEEE Joint Industry Applications Society, Power Electronics and Power Engineering Society chapter, member of the EPE-PEMC council, EPE member and also member of international steering committee at numerous conferences.